IEEE Access
Multidisciplinary ⋮ Rapid Review ⋮ Open Access Journal

Received March 12, 2022, accepted March 23, 2022, date of publication March 28, 2022, date of current version April 4, 2022.

Digital Object Identifier 10.1109/ACCESS.2022.3162628

UAV-Aided Transceiver Design for Secure Downlink OW-DFTs-OFDM System: A Multi-User mmWave Application

JOARDER JAFOR SADIQUE[1], SAIFUR RAHMAN SABUJ[2], (Senior Member, IEEE), SHAIKH ENAYET ULLAH[3], SUJOY KUMAR JOARDER[4], AND MASANORI HAMAMURA[5], (Member, IEEE)

[1]Department of Electrical and Electronic Engineering, Begum Rokeya University, Rangpur, Rangpur 5404, Bangladesh
[2]Department of Electronic Engineering, Hanbat National University, Daejeon 34158, South Korea
[3]Department of Electrical and Electronic Engineering, University of Rajshahi, Rajshahi 6205, Bangladesh
[4]Transcom Electronics Ltd., Dhaka 1212, Bangladesh
[5]Graduate School of Engineering, Kochi University of Technology, Kami, Kochi 782-8502, Japan

Corresponding authors: Joarder Jafor Sadique (joarder@brur.ac.bd) and Masanori Hamamura (hamamura.masanori@kochi-tech.ac.jp)

ABSTRACT Unmanned aerial vehicle (UAV)-based communication system design has already attracted substantial interest due to UAV flexibility in deployment, cost effectiveness, and in-built line-of-sight air-to-ground channels. However, there is a persistent issue of security threats associated with the broadcast nature of UAV: physical layer security (PLS) can be introduced to enhance the secrecy performance in that regard. In the system proposed here, the combined effect of 3D fractional-order Liu chaotic system and 3D fractional-order Li chaotic system is introduced to enhance the PLS of the UAV-to-ground communication network. In addition, to reduce multi-user interference (MUI), efficient orthogonal variable spreading factor (OVSF) codes are integrated with a zero forcing (ZF) scheme. Moreover, to improve bit error rate (BER), a combined MUI signal discrimination and ZF signal detection scheme is introduced, strengthened by various channel coding techniques with multi-user beamforming weighting. The numerical outcomes establish the efficacy of the proposed system in terms of PLS and improvement of data rate with signal-to-interference-plus-noise ratio. This approach achieved an out-of-band emission reduction of 119 dB. Furthermore, an improved BER of 1×10^{-4} is achieved in 16-QAM for a signal-to-noise ratio of 6 dB.

INDEX TERMS Millimeter-wave, orthogonal frequency-division multiplexing, orthogonal variable spreading factor, overlap-windowed discrete Fourier transform, physical layer security, unmanned aerial vehicle, zero forcing precoding.

I. INTRODUCTION

As a promising element for future generation mobile networks, millimeter-wave (mmWave) communication with astounding features is emerging. Leveraging very large bandwidths, mmWave communication can accommodate the ever-growing demand for wireless data [1]. However, mmWave signals are highly sensitive to a blockage, which means that communication by ground users (devices) can be intercepted by hills or tall buildings. This challenge can be addressed through the use of easily deployable and mobile unmanned aerial vehicles (UAVs) as an alternative to terrestrial systems. In addition, UAVs are not vulnerable to line-of-sight (LOS) links and are more suitable for mmWave signal transmission. Therefore, deployment of UAVs as a relay network makes seamless connectivity and a wide range of coverage possible. In that light, the effect of UAV-based relay network deployment in mmWave communication is very encouraging [2], [3].

Massive antennas can be accommodated within a small UAV as a result of the short wavelength of mmWave, since small versions of large-scale antennas can be created for shorter wavelength. UAVs can easily shift to more suitable locations to circumvent obstacles and are capable of utilizing mmWave transmission. Furthermore, the major drawbacks of mmWave, such as path loss and blockage, can be reduced by

The associate editor coordinating the review of this manuscript and approving it for publication was Bilal Khawaja.

careful beamforming design [4]. However, the high beamforming gain in massive antenna systems can improve the signal energy in limited-scattering regions [5].

Although the use of UAVs as a relay network promises significant gains, secured transfer of information is very challenging due to the open nature of air-to-ground wireless channels. Leakage of information in signal transmission over wireless LOS channels is always risky and demands substantial attention. Hence, the addressing of security issues is a most important area of concern in UAV communications [6]. However, may not be appropriate for incorporation in UAV systems, since computational complexity in traditional encryption schemes consumes a huge amount of energy, and UAV eavesdroppers can contaminate the transmission and initiate more aggressive attacks on terrestrial networks. Therefore, the development of advanced techniques such as enhancing physical layer security (PLS) to alleviate attacks by malicious UAVs demands serious attention [7]. PLS is actually a useful alternative for securing wireless communication networks. In estimations of the performance of PLS, secrecy capacity and secrecy outage probability are the two basic parameters which can be modeled by a wiretap channel. Applications of advanced 5G technologies such as non-orthogonal multiple access (NOMA), 3D beamforming, and mmWave are introduced in UAV communication system to further upsurge PLS [6]. To intercept the received signal qualities of a malicious eavesdropper, PLS utilizes the intrinsic characteristics of wireless communication channels, including noise, interference, and fading. Furthermore, PLS ensures keyless secure signal transmission by leveraging various signal designs and signal processing methods [8]. UAV communication networks could obtain both secure transmission and energy efficiency by utilizing proper PLS technologies with differential design of the legitimate channel and eavesdropping channel. At present, UAV-aided wireless communication with PLS has gained substantial attention from the research community. In accordance with the different functions of UAVs in secure communication, UAVs can be classified as UAV-involved secure communications and UAV-enabled secure cooperation [9], [10].

In recent times, two fractional order chaotic systems, three-dimension (3D) Liu chaotic system and 3D Li chaotic system (LLCS), have been introduced as PLS measures [11]. It has been verified that those systems exhibit chaotic behavior over a wide range of the fractional-order. Compared to other existing PLS schemes, these newly introduced fractional-order chaotic systems achieve greater applicability of this particular realization for different applications such as dynamic switching, synchronization, and encryption. They also exhibit better cryptographic capability and are highly suitable for provision of an efficient PLS encryption technique.

Cases of application of UAVs, e.g., as flying base stations (BS) and aerial nodes, are considered with attention to issues of security of confidential information. Various case studies have investigated application of the PLS mechanism [8]. In [10], the authors develop a technique for securing transmission at the physical layer and optimizing degrees of freedom by leveraging some unique features of UAVs. In [12], the authors adopt transmit jamming strategy where some of the UAVs in an array direct jamming signals to mislead eavesdroppers. That work also introduces the use of 3D antenna gain in the air-to-ground links. [13] explores the effectiveness of 5G access in drones for such purposes as enhancement of drone corridor radio coverage; optimization of uplink communication; optimization of network lifetime; and precoding to increase PLS. In [14], the authors investigate the operation of multiple UAV-assisted relay and jammers to secure mmWave communication; and derive new closed-form expressions of secrecy outage probability utilizing models of 3D-antenna gain. By incorporating full-duplex UAVs in terrestrial cellular networks, it is possible to achieve multi-antenna transceiver for zero-padded orthogonal frequency division multiplexing (OFDM) systems [15].

Regarding the prevention or countering of both active and passive eavesdropping in UAV communication, the application of various techniques to PLS, e.g., resource allocation, trajectory design, and cooperative UAVs, to fight against both active and passive eavesdropping in UAV communication has been discussed in [6]. To enhance the secrecy rate of non-orthogonal multiple access transmission (NOMA), a technique for optimization of protected zone shape has been proposed [16] at UAV-BS. In [2], the authors explore secrecy communication in simultaneous wireless information and power transfer UAV-assisted relay system at mmWave. In [1], a power allocation technique is proposed, achieved by separating transmit power between precoder and finger-print embedded authentication tag. The authors of [17] propose precoding strategies that can incorporate the channel state information of an eavesdropper and eliminate the need to transmit artificial noise in underloaded situations. As a means to increase secrecy performance, [4] presents a cooperative jamming technique that utilizes destination and an external UAV for interrupting eavesdroppers.

In light of the above studies and to the best of our knowledge, to date no study has worked to develop an orthogonal variable spreading factor (OVSF)-encoded overlap-windowed discrete Fourier transform spreading orthogonal frequency division multiplexing (OW-DFTs-OFDM) system. This paper presents a multi-antenna configured UAV-assisted OVSF-encoded OW-DFTs-OFDM system that leverages integrated UAVs-terrestrial mobile network with various channel coding. The specific contributions of the paper can be summarized as follows-

- To reduce multi-user interference (MUI) along with computational complexity of the precoding technique, we propose a normalized zero forcing (ZF) precoding technique incorporating efficient OVSF codes. The coverage of mmWave signals get reduced due to extensive path loss associated with mmWave frequencies while passing through obstacles. In addition, the enhanced sensitivity of signals in mmWave frequency may also produce large interference.

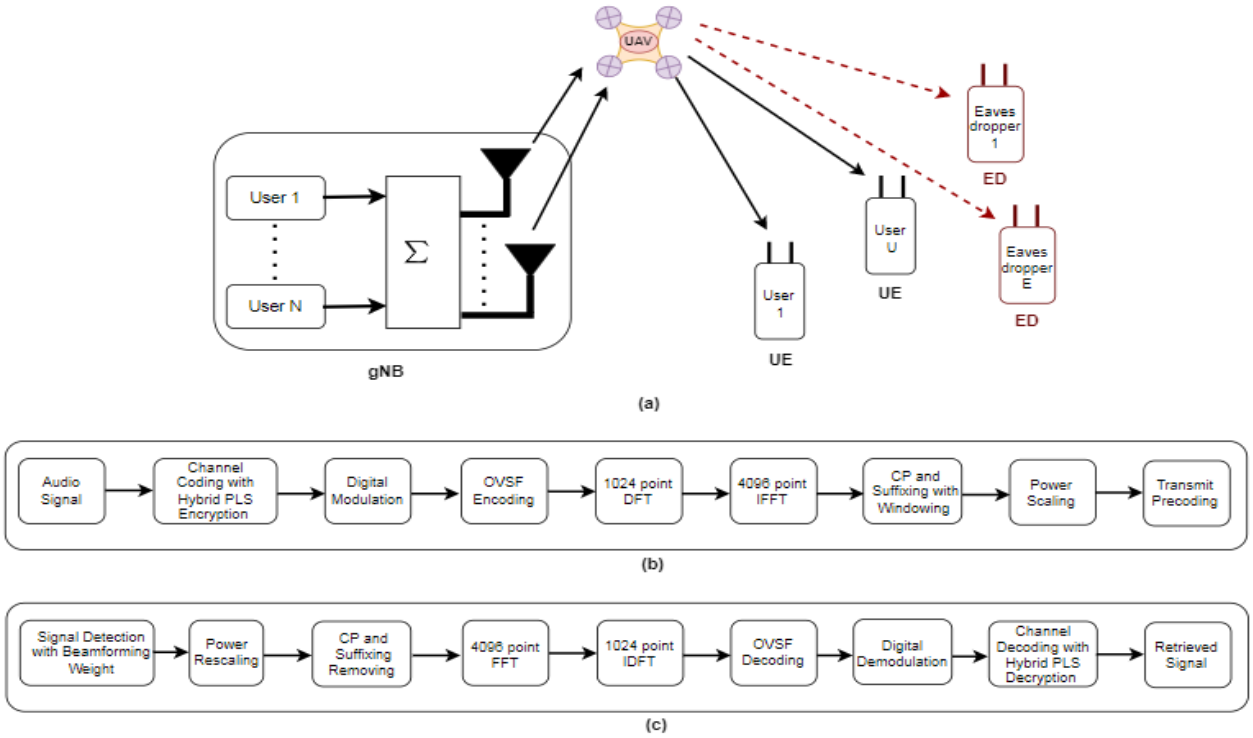

FIGURE 1. **(a) Illustration of the UAV-based relaying wireless networks at mmWave, (b) Transmitter, signal representation for each user in gNB; and (c) Receiver, signal representation in each UE.**

- To achieve the target of minimizing multipath fading channel effects in UAV communication, we introduce null subcarriers in combination with cyclic prefixed (CP) and cyclic suffixed (CS) samples. Compared to the cellular and satellite systems, UAV communication has separate channel characteristics. In general, multipath fading effects are associated with the communication links used by UAVs, which can severely degrade the signal and thus impair communication.
- To minimize out-of-band (OOB) power and at the same time combat spectral leakaging and improve bit error rate (BER) performance, we propose the use of a raised cosine window and a channel coding scheme. One of the major limitations of the OFDM system is OOB interference, which is caused by the sidelobes present in the spectrum of an OFDM symbol. Existing techniques cannot completely reduce the OOB power leakage and thus introduce tremendous degradation of BER performance at the receiver.
- To incorporate the PLS encryption method in our system, we utilize fractional-order based LLCS technique.
- To prove the effectiveness, our proposed system verifies the significant enhancement of user data rate, BER performance, and OOB reduction at reasonably acceptable peak-to-average power ratio (PAPR) by means of a numerical study.

The rest of the paper is organized as follows. Section II presents a system model including network architecture and a signal model. The numerical results are presented in Section III, and concluding remarks and future directions for research are suggested in Section IV.

Notations: In the present study, the notations $|\cdot|^2$, $||\cdot||^2$, $(\cdot)^T$, $(\cdot)^H$ are used to denote the square of the absolute value of complex matrix; the square of the Euclidean norm of complex matrix; the non-conjugate transpose of the complex matrix; and the conjugate transpose of the complex matrix, respectively. The notation $(\cdot)^{-1}$ denotes the inverse of the complex matrix variable.

II. SYSTEM MODEL

A. NETWORK ARCHITECTURE

A UAV-based mmWave relaying network is considered in Fig. 1(a), where a UAV is deployed as a relay to aid transmission from the single next generation base station (gNB) to the U user equipment (UE) and E eavesdropper (ED). The gNB, UEs (legitimate users) and EDs are located on ground and the UAV is located in the sky. Assume that the UAV[1] works in full-duplex[2] using amplify-and-forward (AF) relaying. The total transmission is divided into two time slots. In the first time slot, gNB transmits signals to the UAV; in the second time slot, the UAV forwards the signals to the UEs and EDs.

[1]The UAV receives transmitted signals from gNB and detects the information by means of ZF signal detection technique [18] and sends the detected signals to the UEs.

[2]The authors assume that the self-interference introduced in full-duplex transmission can be perfectly cancelled in a UAV, which may be not realizable in practice. However, it can be eliminated utilizing various interference cancellation methods such as echo canceller, phase conjugate array, retrodirective antenna, and successive interference cancellation at the receiver side [19], [20].

The gNB would be composed of N_T transmitting antennas and it would serve UEs ($\mathcal{U} = 1, 2, \ldots\ldots, U$) via $N_T \times N_T$ a multi-antenna configured UAV. The set of EDs is denoted as $\mathcal{E} = 1, 2, \ldots\ldots, E$. The set of total equipments (i.e., UEs and EDs) is denoted as $\mathcal{U}_t = \mathcal{U} \cup \mathcal{E}$, where $U_t (= U + E)$ is the total number of equipments (devices). Each UE and ED would be equipped with N_R receiving antennas. Fig. 1(a) shows the network architecture, composed of (b) Transmitter and (c) Receiver, described below.

1) TRANSMITTER

On the transmitter side, the extracted binary data from the audio signal of each individual UE are processed with a variety of channel coding schemes such as low density parity check (LDPC), repeat and accumulate (RA), and $\frac{1}{2}$-rated convolutional channel coding schemes [21], [22]. Forward error correction (FEC)-encoded binary data are subsequently encrypted using an LLCS (hybrid PLS) system addressed at [11]. The encrypted binary data are digitally modulated to generate complex symbols [23], which are then encoded with OVSF spreading codes in order to discriminate between the orthogonal spreading sequences of one user and another. Then 1024−point DFT is performed on OVSF spreaded signals and further processed with 4096−point inverse fast Fourier transform (IFFT) to generate DFTs-OFDM signals. Both CP and CS are added to those DFTs-OFDM signals. After that, overlap-windowed (OW) processing is performed using raised cosine window to smooth the transition of amplitude and phase between adjacent DFTs-OFDM blocks [24], [25]. Later the OW-DFTs-OFDM signals are power scaled, processed with a zero forcing precoding scheme [26], and transmitted from the antennas after fixing identical channel power.

2) RECEIVER

On the receiver side, the user's own transmitted signal for each ground UE is detected using respective beamforming weight. The detected signals are power scaled for the purpose of restoring them to their original signal power and then processed to remove cyclic prefixing and suffixing. Then those signals are operated with 4096−point FFT. The FFT operated signals are further processed with 1024−point inverse DFT (IDFT). Later the signals are OVSF despreaded, digitally demodulated, and channel decoded by exploiting hybrid PLS decryption technique to eventually recover audio signals.

B. SIGNAL MODEL

According to [11], the 3D fractional-order Liu chaotic mapping system can be written as

$$D^{q1}[x] = -ax - ey^2 \tag{1a}$$
$$D^{q2}[y] = by - dxz \tag{1b}$$
$$D^{q3}[z] = -cz + mxy, \tag{1c}$$

where q^1, q^2 and q^3 are the fractional orders. a, b, c, e, d, and m are the constant parameters. Using the initial values of (x, y, z) variables, the primary key K_0 of $2049K_U \times 1$ matrix in size can be generated and written as

$$K_0 = \frac{50}{3}\left[|x(t)| + |y(t)| + |z(t)|\right], \tag{2}$$

where $[\cdot]$ indicates the rounding operation to the nearest integer. (50/3) is a multiplication factor value used to confine K_0 values within the desirable range, between 0 and 255. The primary key K_0 is disseminated into U encrypted keys $(K_1, K_2, \ldots\ldots.., K_{U-1}, K_U)$ with each key containing 2049 elements and each element providing eight binary bits.

Using the MATLAB function `repmat`, the length of the binary data of each of the encrypted keys is made identical to the data length of the channel encoded binary data extracted from the audio signal. The encrypted channel encoded binary data vector b_k of data length $\bar{N}$ for user k can be written as

$$\bar{b}_k = b_k \oplus K_k, \tag{3}$$

where $\oplus$ indicates the XOR operation and K_k is the ultimately generated key in binary form using 3D fractional-order Liu chaotic mapping system for user k. The binary data vector $\bar{b}_k$ is further encrypted using 3D fractional-order Li chaotic mapping system based on [11]. That system can be written as

$$D^{q1}[x] = a_1\,(y - x) \tag{4a}$$
$$D^{q2}[y] = (c_1 - a_1) + c_1 y - d_1 xz \tag{4b}$$
$$D^{q3}[z] = b_1 z + e_1 y^2, \tag{4c}$$

where a_1, b_1, c_1, d_1, and e_1 are constant parameters. With consideration of the initial values of (x, y, z) variables, the primary key $\overline{\mathcal{K}}_0$ of $2049K_U \times 1$ matrix in size can be generated and written as

$$\overline{\mathcal{K}}_0 = \frac{20}{3}\left[|x(t)| + |y(t)| + |z(t)|\right], \tag{5}$$

where $[\cdot]$ indicates the rounding operation to the nearest integer; (20/3) is a multiplication factor value used to confine $\overline{\mathcal{K}}_0$ values in the desirable range; the primary key $\overline{\mathcal{K}}_0$ is disseminated to U users and in the case of such keys in binary form $\overline{\mathcal{K}}_1, \overline{\mathcal{K}}_2, \ldots\ldots\ldots, \overline{\mathcal{K}}_{U-1}, \overline{\mathcal{K}}_U$, the second encrypted binary data vector $\bar{b}_k$ of data length $\bar{N}$ for user k can be expressed as

$$\tilde{b}_k = \bar{b}_k \oplus \overline{\mathcal{K}}_k. \tag{6}$$

With added zeros, the doubly encrypted binary data vector $\tilde{b}_k$ of data length $\bar{N}$ is processed for audio to image conversion and the size of the image is $\tilde{N} \times \tilde{N} \times 3$ pixels. The extracted binary data vector c_k of data length $\tilde{\bar{N}} (= \tilde{N} \times \tilde{N} \times 8)$ is converted into a digitally modulated complex symbol vector $\tilde{c}_k$ with data length $\hat{N}$. Regarding the applicability of OVSF spreading, the new form of the complex data vector is d_k with data length $\hat{\bar{N}} (= 8\hat{N})$. The data vector d_k is rearranged into a data matrix $\bar{D}$ of size $M \times \bar{L}$, where $M (= 1024)$ is the number of samples of 1024−point DFT blocks in each column and $\bar{L}$ is the number of columns. The column data vector $\bar{d}_{k,l}$ is

operated with $M-$point DFT and the new data vector $\bar{\bar{d}}_{k,\bar{l}}$ of sample length M for user k can be expressed as

$$\bar{\bar{d}}_{k,\bar{l}}[\bar{m}] = \frac{1}{\sqrt{M}} \sum_{\bar{n}=0}^{\bar{n}=M-1} \bar{d}_{k,l}[\bar{n}]\, e^{-\frac{j2\pi \bar{n}\bar{m}}{M}}, \tag{7}$$

where $\bar{n} = 0, 1, 2, \ldots., M-1$, $\bar{m} = 0, 1, 2, \ldots\ldots., M-1$, and $\bar{l} = 1, 2, \ldots., \bar{L}$.

The DFT operated signal vector presented in Eq. (7) is rearranged into a data matrix $\tilde{D}$ of size $\tilde{N} \times \tilde{L}$, where $\tilde{N}$ is the number of data samples in each column data vector $\bar{d}_{k,l}$ and $\tilde{L}$ is the number of 4096$-$point IFFT blocks. In each data vector $\bar{d}_{k,l}$, $\tilde{\tilde{N}}(= 0.5(N-\tilde{N}))$ zeros are added at each end and the modified form of the column data vector would be $\tilde{\bar{d}}_{k,\bar{l}}$ in a new data matrix $\tilde{\tilde{D}}$ of size $N \times \tilde{L}$. The column data vector $\tilde{\bar{d}}_{k,\bar{l}}$ is operated with $N-$point IFFT and the new data vector $\dddot{d}_{k,l}$ of sample length N for the user k can be written as

$$\dddot{d}_{k,l}[m] = \frac{1}{\sqrt{N}} \sum_{n=0}^{n=N-1} \tilde{\tilde{d}}_{k,l}[n]\, e^{\frac{j2\pi nm}{N}}, \tag{8}$$

where $n = 0, 1, 2, \ldots., N-1$, $m = 0, 1, 2, \ldots\ldots, N-1$, and $l = 1, 2, \ldots., \tilde{L}$. $\tilde{L}$ is the total number of DFT-spread OFDM blocks. On applying CP and CS of sample length CP and CS to the signal model of Eq. (8), we get DFT-spread CP and CS OFDM signal for user k as

$$\dddot{d}_{k,l}[\ddot{m}] = \begin{bmatrix} \frac{1}{\sqrt{N}} \sum_{n=N-CP}^{n=N-1} \tilde{\tilde{d}}_{k,l}[n]\, e^{\frac{j2\pi n\hat{m}}{N}} \\ \frac{1}{\sqrt{N}} \sum_{n=0}^{n=N-1} \tilde{\tilde{d}}_{k,l}[n]\, e^{\frac{j2\pi nm}{N}} \\ \frac{1}{\sqrt{N}} \sum_{n=0}^{n=CS-1} \tilde{\tilde{d}}_{k,l}[n]\, e^{\frac{j2\pi n\check{m}}{N}} \end{bmatrix}, \tag{9}$$

where $\ddot{m} = 0, 1, 2, \ldots., \tilde{N}(= N + CP + CS - 1)$, $l = 1, 2, \ldots\ldots., \tilde{L}$, $\hat{m} = N - CP, \ldots., N-1$, $m = 0, 1, \ldots\ldots, N-1$ and $\check{m} = 0, 1, \ldots\ldots, CS-1$. A raised cosine window is applied at each end of DFT-spread CP and CS OFDM signal vector $\dddot{d}_{k,l}$ for an identical sample length of $CS(= 0.5CP)$ [24]. The overlap-windowed-DFTs-OFDM signal vector is represented by $\tilde{\tilde{d}}_{k,l}$, such that $E\left[\left|\tilde{\tilde{d}}_{k,l}\right|^2\right] = 1$ and the power rescaled signal vector of unity power is represented by $\tilde{\bar{d}}_{k,l}$. On concatenating all the signal vectors $\tilde{\bar{d}}_{k,l}$ for user k, a data matrix D_k is formed, which is $\tilde{N} \times \tilde{L}$ in size.

The 3D distance $d_{(0,k)}$ between the UAV and the UE k with its 3D coordinates $[x_0, y_0, z_0]$ and $[x_k, y_k, z_k]$ can be written as: $d_{0,k} = \sqrt{(x_0-x_k)^2 + (y_0-y_k)^2 + (z_0-z_k)^2}$ and $\theta_{0,k} = \frac{180}{\Pi} \times \sin^{-1}\left(\frac{(z_0-z_k)}{d_{0,k}}\right)$.

On the basis of elevation angle, carrier frequency and environmental factors, the LOS probability from UAV to UE communication can be written, for the case of user k, as [27]

$$P_{LOS}^{0k} = \frac{1}{1 + \Psi \exp\left(-\beta_0\left[\theta_{0,k} - \Psi\right]\right)}, \tag{10}$$

where Ψ and β_0 are the function of environment characteristic. The path loss between the UAV and the UE k can be expressed as [28]:

$$L_{0,k} = \begin{cases} \eta_1 \left(\frac{4\pi f_c d_{0,k}}{c}\right)^{\alpha}, & LOS\ Link \\ \eta_2 \left(\frac{4\pi f_c d_{0,k}}{c}\right)^{\alpha}, & NLOS\ Link \end{cases} \tag{11}$$

where η_1 and η_2 are the excessive path loss coefficients for LOS and non-LOS links. f_c is the carrier frequency, c is the speed of light and α is the path loss exponent. The average path loss between UAV and UE k can be written as [28]

$$\overline{L}_{0,k} = P_{LOS}^{0k}\eta_1 \left(\frac{4\pi f_c d_{0,k}}{c}\right)^{\alpha} + P_{NLOS}^{0k}\eta_2 \left(\frac{4\pi f_c d_{0,k}}{c}\right)^{\alpha}, \tag{12}$$

where $P_{NLOS}^{0k} = 1 - P_{LOS}^{0k}$.

In uplink transmission from gNB with its 3D coordinates $[x_g, y_g, z_g]$ to the UAV, the path loss L_0 for the multiple-input multiple-output (MIMO) flat fading channel H_0 can be expressed as [28]

$$L_0 = P_{LOS}^{go}\, \eta_1 \left(\frac{4\pi f_c d_{g,0}}{c}\right)^{\alpha}, \tag{13}$$

where $d_{0,g} = \sqrt{(x_0-x_g)^2 + (y_0-y_g)^2 + (z_0-z_g)^2}$ and $\theta_{0,g} = \frac{180}{\Pi} \times \sin^{-1}\left(\frac{(z_0-z_g)}{d_{0,g}}\right)$.

MIMO flat fading channels from UAV to UEs are estimated on the basis of the signal models presented in Eq. (12), The total MIMO flat fading channel matrix H of size $N_T \times N_T$ for all the UEs can be formulated as

$$H = \left[H_1^T,\ H_2^T, \ldots\ldots\ldots\ldots, H_{M-1}^T,\ H_M^T\right]^T, \tag{14}$$

As each UE is equipped with N_R receiving antennas, and beam forming weighting requires reshaping of data matrix D_k: all of its elements are stacked into a single column vector and then converted into a matrix $\bar{D}_k$ of size $N_R \times N_C$, where $N_C = (\tilde{N} \cdot \tilde{L})/N_R$. The transmit precoders/beam forming weights (W_k) of k UE can be estimated from the probabilistic path loss model based 3D geometrical MIMO fading channels existing between the UAV and the UEs. For ZF precoding/beamforming weighting, the ZF precoder can be written as [26]

$$\begin{aligned} W_{ZF} &= H^H \left(HH^T\right)^{-1} \\ &= \left[\overline{W}_1,\ \overline{W}_2, \ldots\ldots\ldots., \overline{W}_{U-1},\ \overline{W}_U\right], \end{aligned} \tag{15}$$

where $\overline{W}_1$, $\overline{W}_2$, $\overline{W}_{U-1}$, and $\overline{W}_U$ are the estimated transmit precoders, each of which is an $N_T \times N_R$ matrix. It is noteworthy that at this stage, application of the transmit precoder to input data presents a large amount of signal power; in this paper, we normalize each transmit precoder such that the reestimated transmit precoders for the UE k can be expressed as

$$W_k = \overline{W}_k / \left\|\overline{W}_k\right\|. \tag{16}$$

The transmit precoded signal without power scaling from gNB can be written as

$$X_0 = \sum_{i=1}^{U} W_i X_i. \tag{17}$$

Due to precoding, signal power varies from gNB-UAV channel to UAV-UEs channel. The transmit precoded signal X_0 is to be multiplied by a signal power P_x assigned in $N_T \times N_T$ diagonal dominated matrix such that, transmitted power of all transmitting channels of gNB will be identical and equal to P_g. However, the signal from the gNB received at the UAV can be written as

$$Y_0 = H_0\sqrt{P_x}X_0 + n_0, \tag{18}$$

where $n_0 \sim \mathcal{CN}\left(0_{N_T}, \sigma_0^2 I_{N_T}\right)$ denotes the additive white Gaussian noise (AWGN). On application of ZF signal detection technique addressed at [18], the decoded transmitted signal can be written as

$$\begin{aligned}\ddot{X}_0 &= \left(H_0^H H_0\right)^{-1} H_0^H Y_0 \\ &\cong \sqrt{P_x}X_0.\end{aligned} \tag{19}$$

The signal model presented in Eq. (18) is rescaled to make it compatible with desirable UAV transmission power P_0 of matrix size $N_T \times N_T$, by multiplying with the signal power P_y assigned in an $N_T \times N_T$ diagonal dominated matrix, and the power scaled transmitted signal from the UAV to the UE can be written as

$$\begin{aligned}\dddot{X}_0 &= \sqrt{P_y}\sqrt{P_x}X_0 \\ &= \sqrt{P_x P_y}X_0.\end{aligned} \tag{20}$$

The signal received at the UE k can be expressed as

$$\begin{aligned}Y_k &= H_k\sqrt{P_x P_y}X_0 + n_k \\ &= H_{keq}X_0 + n_k,\end{aligned} \tag{21}$$

where $n_k \sim \mathcal{CN}\left(0_{N_R}, \sigma_k^2 I_{N_R}\right)$ denotes the AWGN and $H_{keq} = H_k\sqrt{P_x P_y}$ is the equivalent channel and it is an $N_R \times N_T$ matrix. The equivalent channel matrix H_{keq} is found to be generally sparse in nature and due to the sparsity of its matrix, its pseudo inverse operation for achieving an exact solution to signal model presented in Eq. (21) cannot be obtained. Using regularized ZF equalization technique to invert the effect of the channel H_{keq} [29], the noise contaminated detected signal for UE k can be written as

$$\begin{aligned}S_k &= \left(H_{keq}^H H_{keq} + \epsilon I_{NT}\right)^{-1} H_{keq}^H Y_k \\ &= \left(H_{keq}^H H_{keq} + \epsilon I_{NT}\right)^{-1} H_{keq}^H H_{keq}X_0 \\ &\quad + \left(H_{keq}^H H_{keq} + \epsilon I_{NT}\right)^{-1} H_{keq}^H n_k \\ &\cong X_0 + n_{\bar{k}},\end{aligned} \tag{22}$$

where $n_{\bar{k}} \sim \mathcal{CN}\left(0_{N_T}, \sigma_{\bar{k}}^2 I_{N_T}\right)$ denotes the AWGN and $\epsilon = 1 \times 10^{-22}$ is the regularization parameter. The signal model of Eq. (22) is further multiplied by user's own channel matrix H_k and we get

$$\begin{aligned}\dddot{S}_k &= H_k S_k \\ &= H_k X_0 + H_k n_{\bar{k}} \\ &= H_k W_k X_k + H_k \sum_{i=1, i\neq k}^{U_t} W_i X_i + n_{\hat{k}},\end{aligned} \tag{23}$$

where $n_{\hat{k}} \sim \mathcal{CN}\left(0_{N_R}, \sigma_{\hat{k}}^2 I_{N_R}\right)$ denotes the AWGN. In Eq. (23), $\|H_k W_k\|^2$ is the instantaneous total signal power for the UE k and $\|H_k W_i\|^2$ is the total instantaneous interference signal power for the UE k and $N_R\sigma_{\hat{k}}^2$ is the AWGN.

For the case of ED, the signal received with its considered channel H_e can be written as

$$\begin{aligned}Y_e &= H_e\sqrt{P_x P_y}X_0 + n_e \\ &= H_{eeq}X_0 + n_e,\end{aligned} \tag{24}$$

where $n_e \sim \mathcal{CN}\left(0_{N_R}, \sigma_e^2 I_{N_R}\right)$ denotes the AWGN and $H_{eeq} = H_e\sqrt{P_x P_y}$ is the equivalent channel. The noise contaminated detected signal for ED can be written as

$$\begin{aligned}S_e &= \left(H_{eeq}^H H_{eeq} + \epsilon I_{NT}\right)^{-1} H_{eeq}^H Y_e \\ &= \left(H_{eeq}^H H_{eeq} + \epsilon I_{NT}\right)^{-1} H_{eeq}^H H_{eeq}X_0 \\ &\quad + \left(H_{eeq}^H H_{eeq} + \epsilon I_{NT}\right)^{-1} H_{eeq}^H n_e \\ &\cong X_0 + n_{\bar{e}},\end{aligned} \tag{25}$$

where $n_{\bar{e}} \sim \mathcal{CN}\left(0_{N_T}, \sigma_{\bar{e}}^2 I_{N_T}\right)$ denotes the AWGN.

By further multiplying the signal model presented in Eq. (25) by ED's own channel matrix H_e, we get

$$\begin{aligned}\dddot{S}_e &= H_e S_e \\ &= H_e X_0 + H_e n_{\bar{e}} \\ &= H_e W_k X_k + H_e \sum_{i=1, i\neq k}^{U_t} W_i X_i + n_{\ddot{e}},\end{aligned} \tag{26}$$

where $n_{\ddot{e}} \sim \mathcal{CN}\left(0_{N_R}, \sigma_{\ddot{e}}^2 I_{N_R}\right)$ denotes the AWGN. In Eq. (26) the value of $H_e W_k X_k$ is very much negligible and the ED would only receive noisy signal.

The received signal-to-interference-plus-noise ratio (SINR) for the UE k after ZF precoding based decoding can be written as

$$SINR_k = \frac{\|H_k W_k\|^2}{\sum_{i=1, i\neq k}^{U_t} \|H_k W_i\|^2 + N_R\sigma_{\hat{k}}^2}. \tag{27}$$

The data rate for UE k can be written as [30]

$$R_k = B\log_2(1 + SINR_k), \tag{28}$$

where B is the channel bandwidth.

C. BER CALCULATION ALGORITHM

The main steps of calculating BER in our proposed system are presented in **Algorithm 1** provided below:

Algorithm 1 BER Calculation

1. **Input:** Initial parameters provided in Table 1 and BER = 0;
2. **for all** $k \in \mathcal{U}$ **do**
3. Generate random data b_k for UE k;
4. Generate primary key K_0 using Eqs. (1) and (2);
5. First encryption: Encrypt binary data $\overline{b}_k = b_k \oplus K_k$ using Eq. (3);
6. Generate primary key $\overline{\mathcal{K}}_0$ using Eqs. (4) and (5);
7. Second encryption: Encrypt binary data $\tilde{b}_k = \overline{b}_k \oplus \overline{\mathcal{K}}_k$ using Eq. (6);
8. Execute digital modulation and OVSF encoding;
9. Execute $M-$point DFT using Eq. (7);
10. Execute $N-$point IFFT using Eq. (8);
11. Obtain OFDM signal applying CP and CS given Eq. (9);
12. Transmit precoded signal X_0 without power scaling from gNB given Eq. (17);
13. Receive signal Y_0 at the UAV given Eq. (18);
14. Decode signal $\ddot{X}_0$ and power scale signal $\dddot{X}_0$ to transmit from the UAV given Eqs. (19) and (20);
15. Receive signal Y_k at the UE k;
16. Detect signal $\ddot{S}_k$ for UE k using Eq. (23);
17. Remove CP and CS from $\ddot{S}_k$;
18. Execute $N-$point FFT and $M-$point IDFT;
19. Execute OVSF decoding and digital demodulation;
20. Second and first decryption: Decrypt binary data b_k^d;
21. BER = BER + sum(not($b_k^d == b_k$));
22. **end for**
23. **Output:** BER;

D. COMPUTATIONAL COMPLEXITY

In this section, we discuss the computational complexity of the proposed system, as determined by the total number of complex multiplications employed in transmission and reception.

- The number of multiplications and additions for LLCS encryption, $\vartheta_{LLCS} = 8\,N_e K_U + 8\,N_e K_U$, where N_e and K_U are the number of elements contained in each key and total encrypted keys, respectively.
- For OVSF spreading, $\vartheta_{OVSF} = 8\hat{N}$, where $\hat{N}$ is the data length of the digitally modulated complex symbol.
- For DFT operation, $\vartheta_{DFT} = M \times \bar{L}$, where M is the number of samples of M-point DFT and $\bar{L}$ is the number of columns.
- For IFFT operation, $\vartheta_{IFFT} = \tilde{N} \times \tilde{L}$, where $\tilde{N}$ is the data samples in each column data vector and $\tilde{L}$ is the number of N-point IFFT block.
- For OW-DFTs-OFDM operation, $\vartheta_{OW-DFTs-OFDM} = \tilde{N} \times \tilde{L}$, where $\tilde{N}(= N + CP + CS - 1)$ and $\tilde{L}$ is the total number of DFT-spread OFDM block.

The total computational complexity of the proposed system is $\mathcal{O}(\vartheta_{LLCS} + \vartheta_{OVSF} + \vartheta_{DFT} + \vartheta_{IFFT} + \vartheta_{OW-DFTs-OFDM})$. According to [15], the total computational complexity is $\mathcal{O}(\vartheta_{ILM} + \vartheta_{WHT(User)} + \vartheta_{WHT(Eave)} + \vartheta_{PAPR(User)} + \vartheta_{PAPR(Eave)} + \vartheta_{IDFT(User)} + \vartheta_{IDFT(Eave)})$, where ϑ_{ILM} represents the complexity of interwining logistic map (ILM)-cosine transform, $\vartheta_{WHT(User)}$ represents the complexity of walsh-hadamard transform (WHT) of legitimate user, $\vartheta_{WHT(Eave)}$ represents the complexity of WHT of ED, $\vartheta_{PAPR(User)}$ represents the complexity of PAPR of legitimate user, $\vartheta_{PAPR(Eave)}$ represents the complexity of PAPR of ED, $\vartheta_{IDFT(User)}$ represents the complexity of IDFT of legitimate user, and $\vartheta_{IDFT(Eave)}$ represents the complexity of IDFT of ED. So, the proposed system has less computational complexity than the system presented in [15].

TABLE 1. Simulation parameters.

Description	Value
No. of audio samples of each UE	4098
Sampling frequency of audio signal (Hz)	8000
UAV height (m)	120
UAV transmission power (dBm)	30
gNB transmission power (dBm)	46
No. of subcarriers	4096
No. of null subcarriers	796
CP and CS lengths (samples)	512 and 256
Subcarrier spacing (KHz)	60
Channel Bandwidth (MHz)	245.76
Noise power (dBm)	-120
Transmitter at gNB	8
Receiver at UE and ED	2
Signal-to-noise ratio, E_b/N_0 (dB)	$0-20$

III. SIMULATION RESULTS AND DISCUSSION

In this section, the numerical results are presented for the PLS encrypted multiuser mmWave UAV-assisted OVSF-encoded OW-DFTs-OFDM system under the simulation parameters presented in Table 1. Here, a special case of four UEs and one ED is considered. The height of four UEs and single ED is considered to be 1.5 m and are located at a distance of 138 m, 129 m, 122 m, 131 m, and 135 m respectively away from the UAV, and the distance between the gNB (at a height of 50 m) and the UAV (at a height of 120 m) is 158 m. The height of ED and The location of the UAV and the considered number of UEs are assumed to be recognizable to the associates. Generally, it is required that the channel state information (CSI) be estimated by the UEs. However, in practice the transmitting UAV and UEs have different CSI. In such cases, CSI has been obtained from the estimated MIMO flat-fading channel in specific cases of downlink transmission. In this proposed system, we emphasis secure transmission with utilization of LLCS.

In Figure 2, the bifurcation diagrams of the fractional-order Liu system are presented with fractional orders, initial (x, y, z), and parameter (a, b, c, e, d, m) values to [0.9 0.9 0.9], [0.8 1.7 0.5] and [0.5 3.5 5.0 1.1 1.3 7.0]. The estimated 8-bit keys with integer values ranging from 0 to 255 for different users are presented in Figure 3.

In Figure 4, the bifurcation diagrams of the fractional-order Li system are presented with fractional orders, initial (x, y, z), and parameter $(a_1, b_1, c_1, d_1, e_1)$ values to [0.9 0.9 0.9], [0.75 -0.5 0.8] and [4.1 1.0 5.9 2.1 1.5]. The generated 8-bit keys are shown in Figure 5.

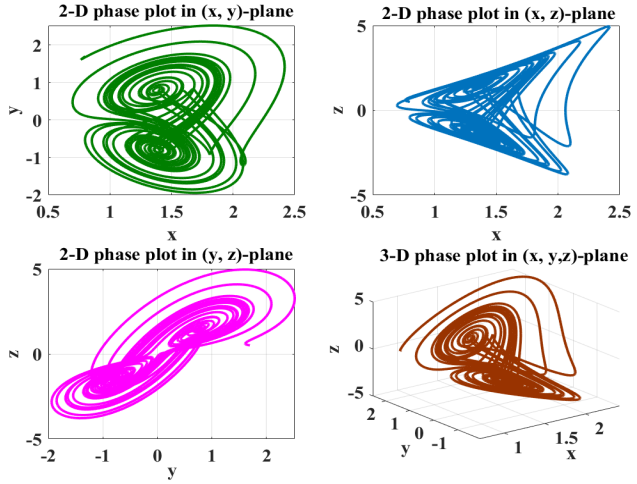

FIGURE 2. Bifurcation diagrams of the commensurate fractional-order Liu system in both 2D and 3D phases.

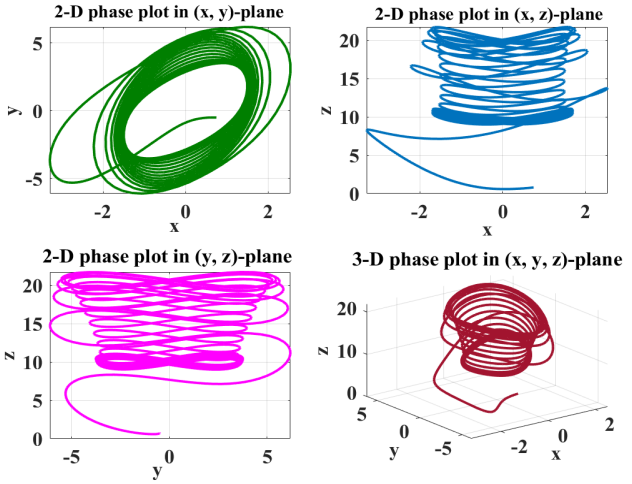

FIGURE 4. Bifurcation diagrams of the commensurate fractional-order Li system in both 2D and 3D phases.

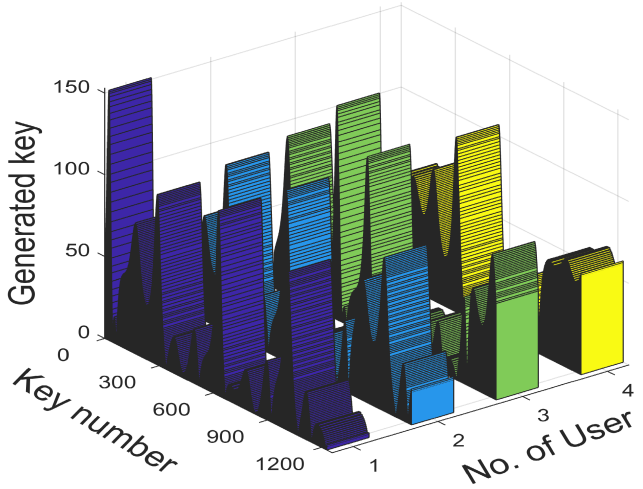

FIGURE 3. Keys for different users, generated using fractional-order Liu system.

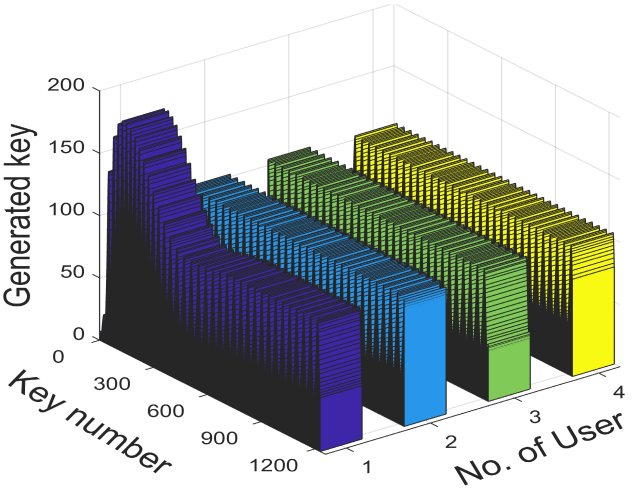

FIGURE 5. Keys for different users, generated using Fractional-order Li system.

To evaluate the LLCS, the LLCS encrypted binary data vector $\bar{b}_k$ and its non-encrypted binary data vector b_k for user k can be converted individually into eight bit decimal integer (symbolic) values and represented by a LLCS encrypted symbolic data vector $\bar{b}_{PLS-k}$ and a non-encrypted symbolic data vector $\bar{b}_{NPLS-k}$. The values of $\bar{b}_{PLS-k}$ and $\bar{b}_{NPLS-k}$ can be determined by using Eq. (6). The effectiveness of the LLCS encryption for ensuring secrecy against passive ED for user k can be written in terms of an estimation of the correlation between $\bar{b}_{PLS-k}$ and $\bar{b}_{NPLS-k}$ as [31]:

$$\text{corr}(\bar{b}_{PLS-k}, \bar{b}_{NPLS-k}) = \frac{\text{cov}(\bar{b}_{PLS-k}, \bar{b}_{NPLS-k})}{\text{SD}(\bar{b}_{PLS-k}) \cdot \text{SD}(\bar{b}_{NPLS-k})}, \quad (29)$$

where $\text{cov}(\bar{b}_{PLS-k}, \bar{b}_{NPLS-k}) = \frac{1}{\ddot{n}-1} \sum_{\hat{k}=1}^{\ddot{n}} (\bar{b}_{PLS-k,\hat{k}} - \overline{b_{PLS-k}})(\bar{b}_{NPLS-k,\hat{k}} - \overline{b_{NPLS-k}})$, $\text{SD}(\bar{b}_{PLS-k}) = \frac{1}{\ddot{n}-1} \sum_{\hat{k}=1}^{\ddot{n}} (\bar{b}_{PLS-k,\hat{k}} - \overline{b_{PLS-k}})$, and $\text{SD}(\bar{b}_{NPLS-k}) = \frac{1}{\ddot{n}-1} \sum_{\hat{k}=1}^{\ddot{n}} (\bar{b}_{NPLS-k,\hat{k}} - \overline{b_{NPLS-k}})$. The number of LLCS encrypted/non-encrypted symbolic data vectors and their lengths are $\ddot{n} (= \bar{N}/8)$ and $\hat{k} = 1, 2, \ldots\ldots \ddot{n}$, respectively. $\overline{b_{PLS-k}}$ and $\overline{b_{NPLS-k}}$ are the mean values of the $\bar{b}_{PLS-k}$ and $\bar{b}_{NPLS-k}$, respectively. The symbolic notations $\bar{b}_{PLS-k,\hat{k}}$ and $\bar{b}_{NPLS-k,\hat{k}}$ are the $\hat{k}$-th elements of the symbol vectors $\bar{b}_{PLS-k}$ and $\bar{b}_{NPLS-k}$, respectively. $\text{cov}(X_1, X_2)$ and $\text{corr}(X_1, X_2)$ represent the covariance and correlation of two random variables X_1 and X_2, respectively. $\text{SD}(\cdot)$ is the standard deviation.

Using Eq. (29), it is observable that LLCS encryption scheme has a significant impact on generated symbolic integer values in Figure 6. The estimated correlation value with and without implementation of the LLCS encryption scheme for user k is found to have a value of 0.0486, which is clearly indicative of significant dissimilarity between the symbolic data.

Figure 7 shows that the data (information) of the four users are totally hidden and encrypted by means of an audio-to-image transformation scheme utilizing simultaneous implementation of LLCS based PLS encryption techniques.

It can be seen in Figure 8 that the OOB power reduction of 95.99 dB, 94.96 dB, 95.16 dB, and 93.22 dB are achieved with CP sample length of 128 for user 1, user 2, user 3 and

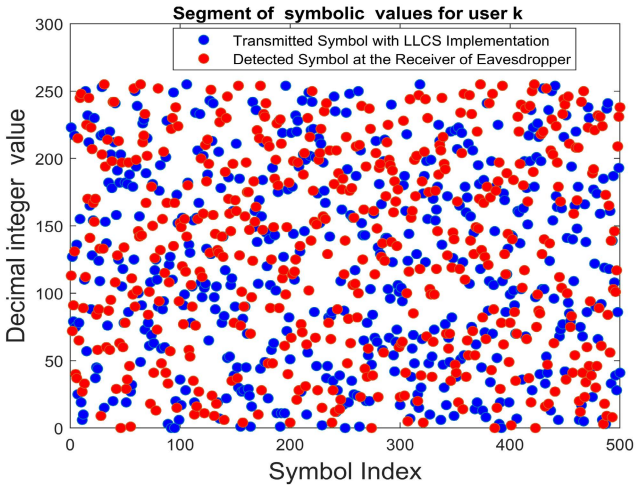

FIGURE 6. Comparison between transmitted symbol of user *k* and received symbol of ED.

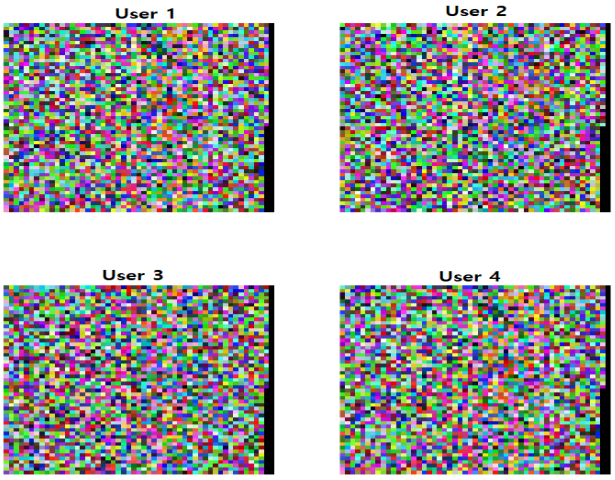

FIGURE 7. Audio converted to images for different users with implementation of LLCS based PLS encryption schemes.

user 4, respectively. By increasing CP sample length from 128 to 256, power reduction of 107.94 dB, 106.21 dB, 106.16 dB and 105.97 dB respectively are obtained for the individual users considered here. Again, further enhancement of CP sample length to 512, i.e. improved OOB power reduction of 119.84 dB, 118.34 dB, 119.59 dB, and 118.97 dB are achieved for user 1, user 2, user 3 and user 4, respectively.

Figure 9 shows the PAPR reduction performance of the proposed system, presented by means of the complementary cumulative distribution function (CCDF). It is noteworthy that the PAPR of the transmitted signal with DFT spreading is about 2.5 dB lower than in the system without DFT spreading technique at a CCDF value of 1×10^{-3}.

In Figure 10, graphical representations of transmitted audio signals of different users are presented without utilizing the LLCS scheme. Due to implementation of the LLCS scheme, waveforms of the individual users are totally changed, as depicted in Figure 11.

In Figure 12, the retrieved audio signals contain a significant amount of noise at E_b/N_0 value of 0 dB; such signals

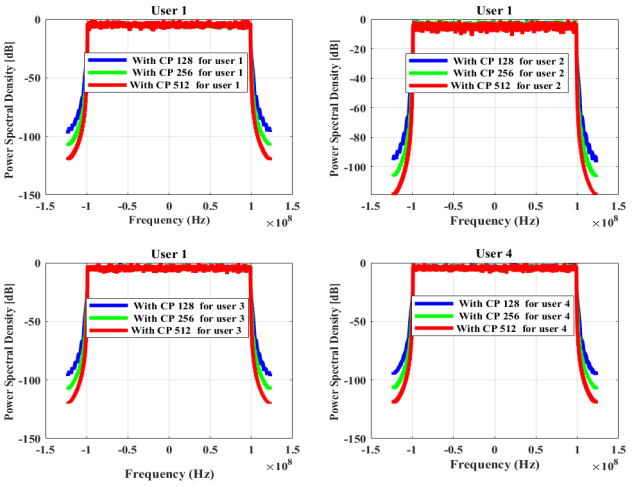

FIGURE 8. Estimated power spectral density for different users with varying CP.

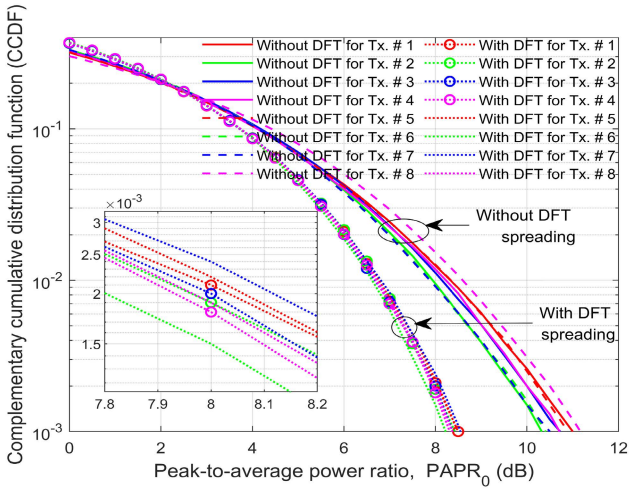

FIGURE 9. Impact of DFT spreading at eight transmitting antenna ports of gNB on CCDFs of PAPR for the proposed system.

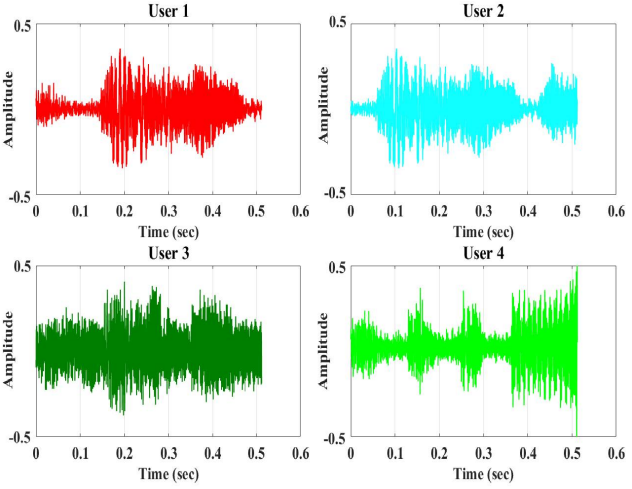

FIGURE 10. Transmitted audio signal of different users without implementation of LLCS.

do not have any similarities to those presented in Figure 10. In Figure 13, the retrieved audio signals at E_b/N_0 value of 10 dB have significant and satisfactory similarities with the

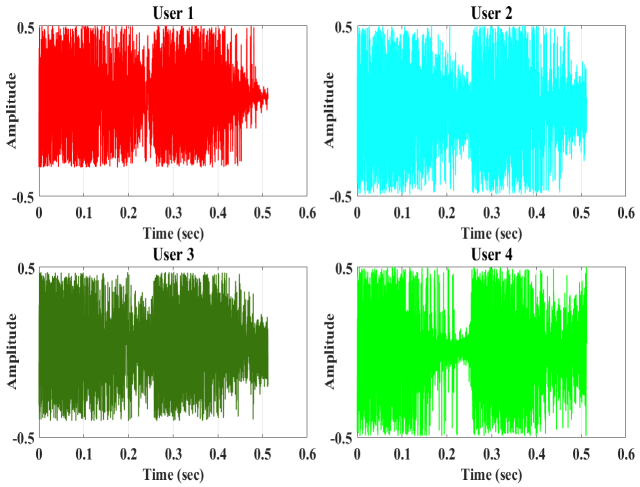

FIGURE 11. Transmitted audio signal of different users with implementation of LLCS.

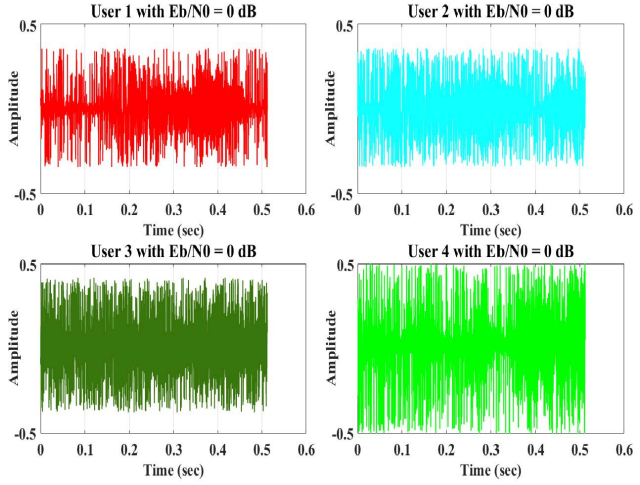

FIGURE 12. Retrieved audio signal of different users in LLCS implemented with E_b/N_0 value of 0 dB.

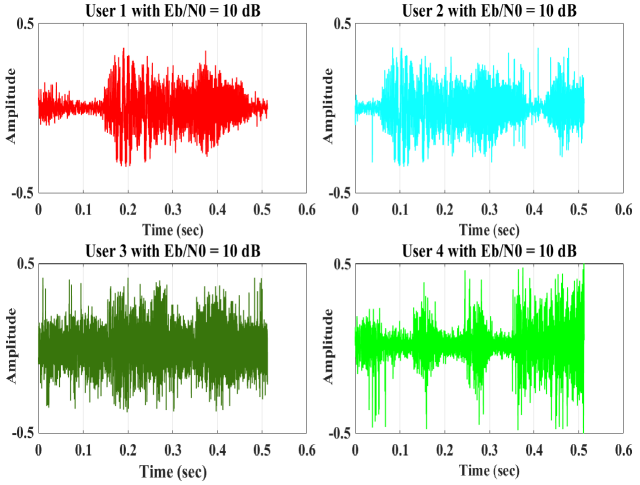

FIGURE 13. Retrieved audio signal of different users in LLCS implemented with E_b/N_0 value of 10 dB.

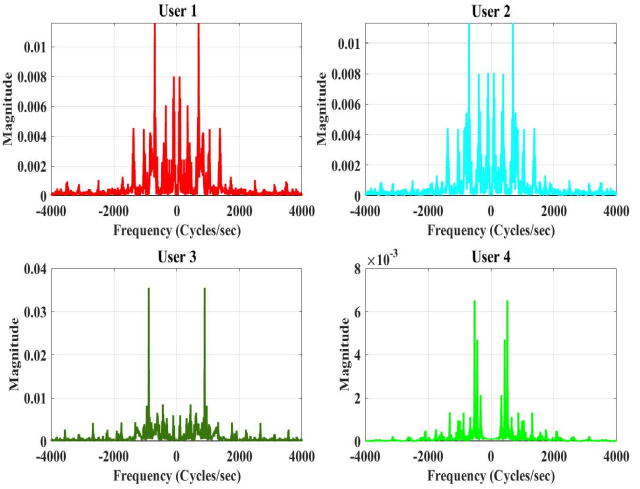

FIGURE 14. Power spectrum of transmitted audio signals for different users.

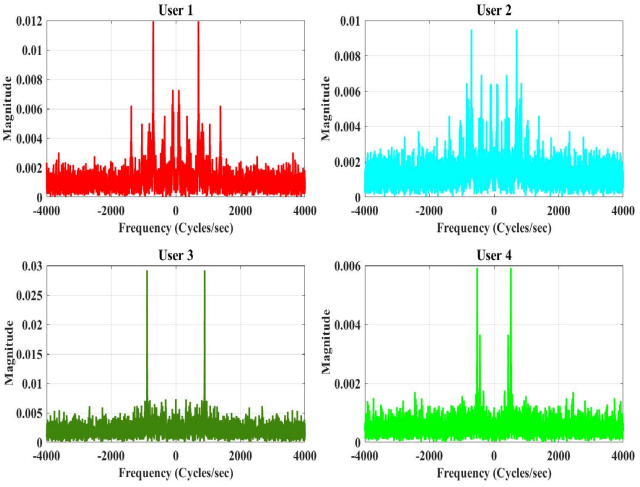

FIGURE 15. Power spectrum of retrieved audio signals for different users at E_b/N_0 value of 0 dB.

transmitted signals presented in Figure 10, with the adoption of LDPC channel coding and 16-QAM digital modulation technique at an estimated BER of zero.

In Figures 14 through 16, the power spectra of transmitted and retrieved audio signals at E_b/N_0 values of 0 dB and 10 dB are presented for different users. The estimated power at different frequency components is found to be identical in the case of transmitted audio signals and retrieved signals at E_b/N_0 value of 10 dB (Figures 14 and 16). In case of noise contamination at E_b/N_0 value of 0 dB (Figure 15), the scenario is completely changed and that effect dominates throughout the whole frequency band. In the proposed system, multiple antennas are preferably used at both the transmitter and the receiver, in order to exploit the spatially diverse communication link. In addition, the implementation of precoding based MIMO beamforming technique combined with OVSF spreading codes presents uncorrelated received signals and also improves SINR and data rate. The estimated received SINR values are presented with respect to the E_b/N_0 values in Figure 17, which indicate that the quality of the received signals is good and the estimated data rate is also reasonably acceptable, as can be seen in Figure 18.

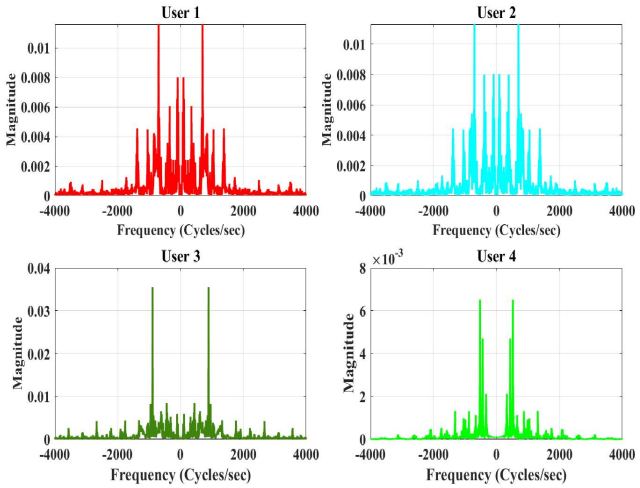

FIGURE 16. Power spectrum of retrieved audio signals for different users at E_b/N_0 value of 10 dB.

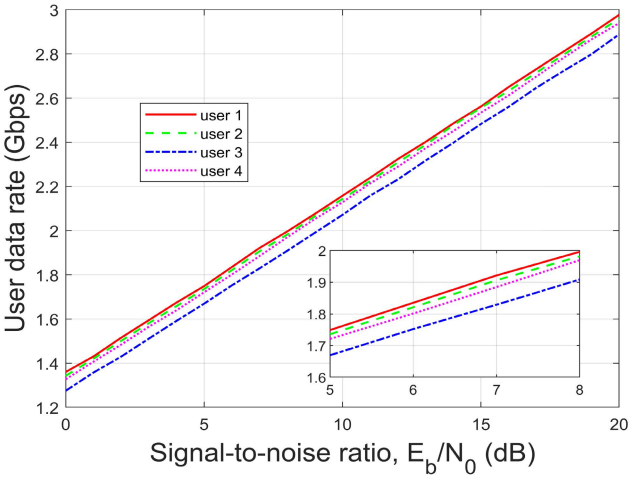

FIGURE 18. Estimated user data rate for different users at varying E_b/N_0 values.

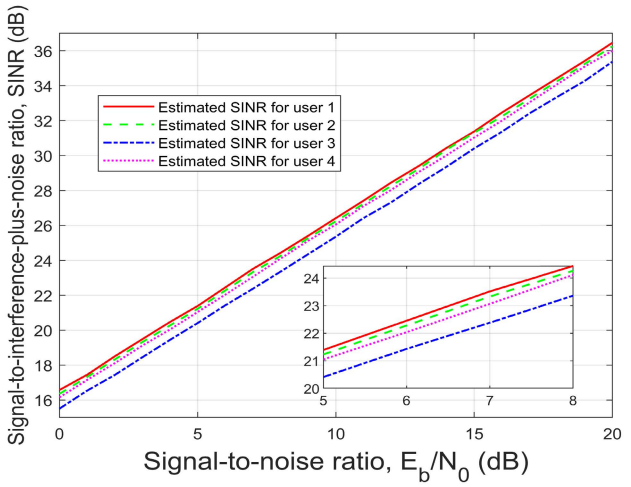

FIGURE 17. Estimated received SINR for different users at varying E_b/N_0 values.

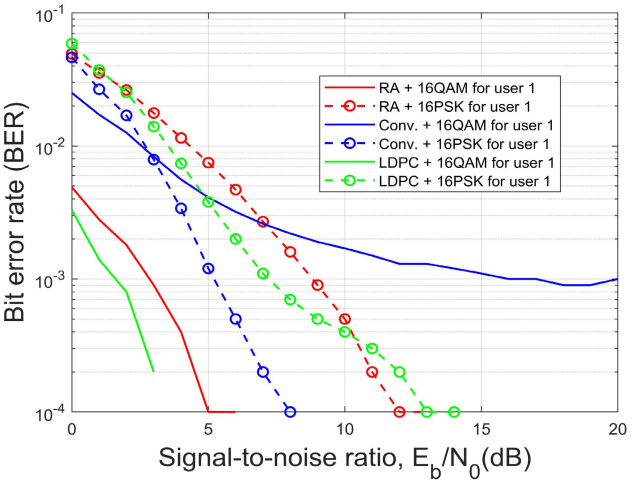

FIGURE 19. Changes in BER as a function of E_b/N_0 under the proposed system for user 1.

Figures 19 through 22 show the BER results under different system configurations for all users. It is clearly visible that in all cases, the simulated system performs comparatively better under LDPC channel coding technique. For the case of user 1, the BER varies from 2.64% to 0.08% for 16-PSK with RA channel coding and 16-QAM with LDPC, respectively, for assumed typical E_b/N_0 values of 2 dB, as shown in Figure 19. At 0.1% BER, an E_b/N_0 gain of 7 dB is achieved in 16-QAM with LDPC, in contrast to 16-PSK with RA channel coding.

In Figure 20, it can be seen that for user 2, the BER varies from 4.80% to 0.20% in the case of 16-PSK and 16-QAM utilizing LDPC channel coding technique for assumed typical E_b/N_0 values of 2 dB. For the customarily acceptable E_b/N_0 values of 5 dB, the estimated BER values are 0.00014 and 0.02478 in the case of 16-QAM with LDPC and 16-PSK with RA, respectively, which verifies a system performance improvement of 22.48 dB.

It is noteworthy that in Figure 21 the BER varies from 10.73% to 0.37% in the case of 16-PSK with $\frac{1}{2}$-rated convolutional channel coding and 16-QAM with LDPC channel coding at an E_b/N_0 value of 2 dB for user 3. For the considered E_b/N_0 value of 5 dB, the estimated BER values are 0.0002 and 0.0460 respectively in the case of 16-QAM with LDPC and 16-PSK with RA channel coding, which correspond to a significant system performance improvement of 23.62 dB.

In the case of user 4, it can be seen in Figure 22 that the BER varies from 5.46% to 0.17% for 16-PSK with RA channel coding and 16-QAM with LDPC channel coding at an E_b/N_0 value of 2 dB. For the customarily acceptable E_b/N_0 value of 5 dB, the estimated BER values are 0.0001 and 0.0290 respectively for 16-QAM with LDPC and 16-PSK with RA channel coding, which verifies a system performance improvement of 24.63 dB.

In Figure 23, the BER performance of the proposed system is compared with that of various other schemes. For further details, a brief discussion is included on utilized schemes presented by the authors in [32]–[35]. The authors of [32] generalized the Nyquist criteria for ordinary linear modulation to the discrete-Fourier transform (DFT) spread OFDM

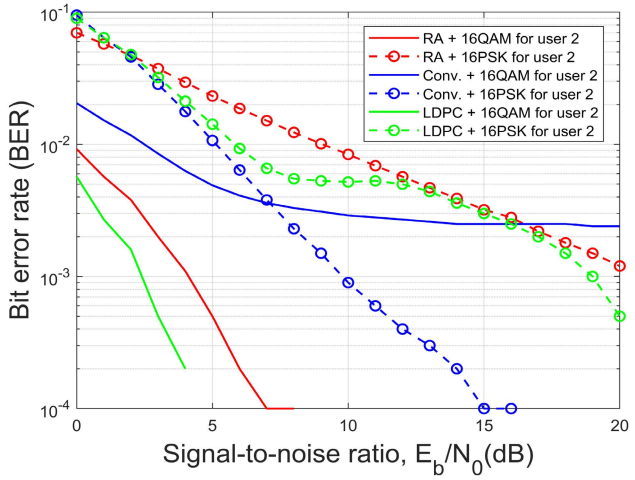

FIGURE 20. Changes in BER as a function of E_b/N_0 under the proposed system for user 2.

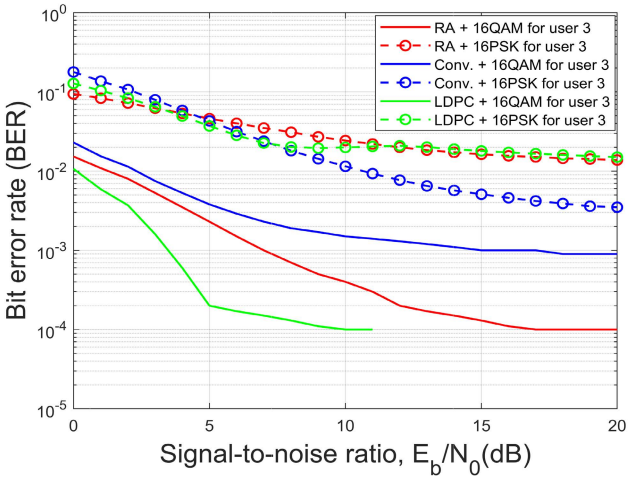

FIGURE 21. Changes in BER as a function of E_b/N_0 under the proposed system for user 3.

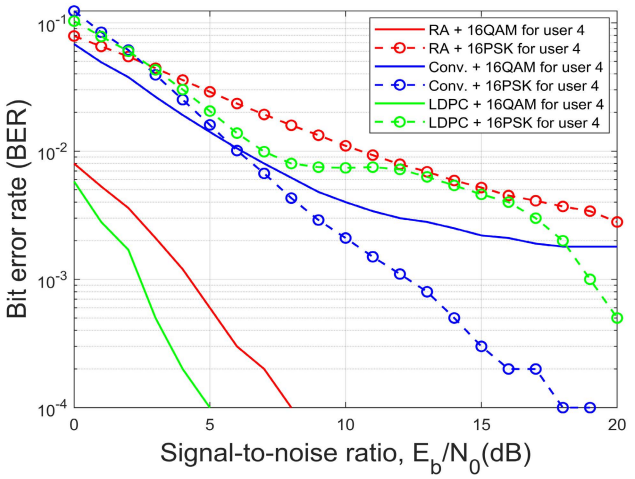

FIGURE 22. Changes in BER as a function of E_b/N_0 under the proposed system for user 4.

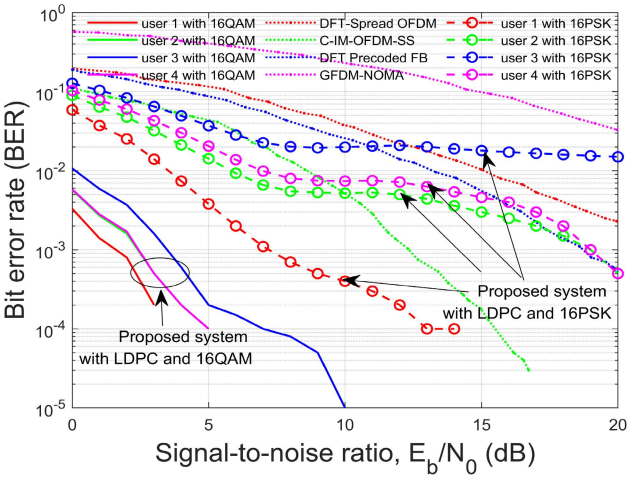

FIGURE 23. Comparative analysis of the proposed system with other multicarrier systems in terms of BER performance.

of constellation-rotated pulse amplitude modulation symbols. In [33], the authors propose an OFDM scheme which incorporates index modulation, spread spectrum, and C-transform techniques and strongly emphasizes the BER performance of the proposed OFDM, conventional OFDM systems, and several other similar systems. The authors of [34] propose a new precoded filter bank system based on the pruned DFT spread filter bank multicarrier modulation scheme utilizing only the notion of double rate transmission in combination with a data allocation strategy. In that scheme, both BER performance and PSD comparison between filters are presented. In [35], the authors combined a generalized frequency division multiplexing (GFDM) system with a power-domain NOMA system, and present numerical results indicating improved BER and higher achievable sum rate with lower PAPR and OOB power radiation.

The proposed scheme clearly outperforms all the other schemes under 16-QAM and LDPC channel coding technique, as shown in Figure 23. With the exception of user 3, the BER of all the users became 0 after E_b/N_0 value of 5 dB.

TABLE 2. Comparison of BER of various schemes, at $E_b/N_0 = 6$ dB.

Schemes	BER
[32]	0.0834
[33]	0.0227
[34]	0.0636
[35]	0.3435
Proposed (16-PSK)	0.0283
Proposed (16-QAM)	0.0002

The BER of users 2 and 4 are almost identical throughout the E_b/N_0 range of $0-5$ dB. As a consequence, it can be stated with confidence that in terms of BER performance, the proposed multi-user OW-DFTs-OFDM system under 16-QAM and LDPC channel coding technique is more robust than the other similar systems presented above. Even the BER of user 1 demonstrates relatively better performance for the case of the proposed system adopting 16-PSK digital modulation. Considering the typical assumed value of $E_b/N_0 = 6$ dB, the BERs of the proposed scheme for arbitrarily chosen cases of user 3 and all other systems is shown in Table 2.

IV. CONCLUSION AND FUTURE WORK

We have investigated an UAV-assisted mmWave downlink OVSF-encoded OW-DFTs-OFDM system for secured data transmission. In this study, the implementation of OVSF spreading code and ZF precoding in UAV-aided mmWave OW-DFTs-OFDM system resulted in the reduction of MUI and the enhancement of the user data rate. Our designed system, with null subcarriers inserted at both ends of an OFDM symbol and with utilization of raised cosine filter at both ends of a OW-DFTs-OFDM symbol, has made achieved a satisfactory reduction of OOB spectrum power and elimination of the effect of fading channel at mmWave. We studied the system performance in terms of BER, using various channel coding schemes including LDPC, RA and $\frac{1}{2}$-rated convolutional with 16-QAM and 16-PSK digital modulations. Moreover, the findings show that LDPC channel coding with 16-QAM digital modulation can achieve low BER performance. As for further research on the proposed system, there are still many issues to be studied, notably: (i) the effect of multiple eavesdroppers; (ii) deployment of massive MIMO [36]; (iii) enhancement of the effectiveness of PLS technique [37]; and (iv) incorporation of deep neural networks and other innovative tools [38].

REFERENCES

[1] S. J. Maeng, Y. Yapici, I. Guvenc, H. Dai, and A. Bhuyan, "Power allocation for fingerprint-based PHY-layer authentication with mmWave UAV networks," in *Proc. IEEE Int. Conf. Commun.*, Jun. 2021, pp. 1–6.

[2] X. Sun, W. Yang, Y. Cai, R. Ma, and L. Tao, "Physical layer security in millimeter wave SWIPT UAV-based relay networks," *IEEE Access*, vol. 7, pp. 35851–35862, 2019.

[3] A. R. Rahul, S. R. Sabuj, M. S. Akbar, H.-S. Jo, and M. A. Hossain, "An optimization based approach to enhance the throughput and energy efficiency for cognitive unmanned aerial vehicle networks," *Wireless Netw.*, vol. 27, no. 1, pp. 475–493, Jan. 2021.

[4] X. Pang, M. Liu, N. Zhao, Y. Chen, Y. Li, and F. R. Yu, "Secrecy analysis of UAV-based mmWave relaying networks," *IEEE Trans. Wireless Commun.*, vol. 20, no. 8, pp. 4990–5002, Aug. 2021.

[5] A. Koc and T. Le-Ngoc, "Full-duplex mmWave massive MIMO systems: A joint hybrid precoding/combining and self-interference cancellation design," *IEEE Open J. Commun. Soc.*, vol. 2, pp. 754–774, 2021.

[6] X. Sun, D. W. K. Ng, Z. Ding, Y. Xu, and Z. Zhong, "Physical layer security in UAV systems: Challenges and opportunities," *IEEE Wireless Commun.*, vol. 26, no. 5, pp. 40–47, Oct. 2019.

[7] Q. Wu, W. Mei, and R. Zhang, "Safeguarding wireless network with UAVs: A physical layer security perspective," *IEEE Wireless Commun.*, vol. 26, no. 5, pp. 12–18, Oct. 2019.

[8] B. Li, Z. Fei, Y. Zhang, and M. Guizani, "Secure UAV communication networks over 5G," *IEEE Wireless Commun.*, vol. 26, no. 5, pp. 114–120, Oct. 2019.

[9] R. Dong, B. Wang, K. Cao, and T. Cheng, "Securing transmission for UAV swarm-enabled communication network," *IEEE Syst. J.*, early access, Sep. 29, 2021, doi: 10.1109/JSYST.2021.3111746.

[10] H.-M. Wang, X. Zhang, and J.-C. Jiang, "UAV-involved wireless physical-layer secure communications: Overview and research directions," *IEEE Wireless Commun.*, vol. 26, no. 5, pp. 32–39, Oct. 2019.

[11] S. M. Mohamed, W. S. Sayed, L. A. Said, and A. G. Radwan, "Reconfigurable FPGA realization of fractional-order chaotic systems," *IEEE Access*, vol. 9, pp. 89376–89389, 2021.

[12] Y. Zhu, G. Zheng, and M. Fitch, "Secrecy rate analysis of UAV-enabled mmWave networks using Matérn hardcore point processes," *IEEE J. Sel. Areas Commun.*, vol. 36, no. 7, pp. 1397–1409, Jul. 2018.

[13] A. Bhuyan, I. Guvenc, H. Dai, M. L. Sichitiu, S. Singh, A. Rahmati, and S. J. Maeng, "Secure 5G network for a nationwide drone corridor," in *Proc. IEEE Aerosp. Conf.*, Mar. 2021, pp. 1–10.

[14] R. Ma, W. Yang, Y. Zhang, J. Liu, and H. Shi, "Secure mmWave communication using UAV-enabled relay and cooperative jammer," *IEEE Access*, vol. 7, pp. 119729–119741, 2019.

[15] J. J. Sadique, S. E. Ullah, M. R. Islam, R. Raad, A. Z. Kouzani, and M. A. P. Mahmud, "Transceiver design for full-duplex UAV based zero-padded OFDM system with physical layer security," *IEEE Access*, vol. 9, pp. 59432–59445, 2021.

[16] N. Rupasinghe, Y. Yapici, I. Guvenc, H. Dai, and A. Bhuyan, "Enhancing physical layer security for NOMA transmission in mmWave drone networks," in *Proc. 52nd Asilomar Conf. Signals, Syst., Comput.*, Oct. 2018, pp. 729–733.

[17] S. J. Maeng, Y. Yapici, I. Guvenc, H. Dai, and A. Bhuyan, "Precoder design for mmWave UAV communications with physical layer security," in *Proc. IEEE 21st Int. Workshop Signal Process. Adv. Wireless Commun. (SPAWC)*, May 2020, pp. 1–5.

[18] Y. S. Cho, J. Kim, W. Y. Yang, and C. G. Kang, *MIMO-OFDM Wireless Communications With MATLAB*. Hoboken, NJ, USA: Wiley, 2010.

[19] N. Qi, M. Wang, W.-J. Wang, T. A. Tsiftsis, R. Yao, and G. Yang, "Energy efficient full-duplex UAV relaying networks under load-carry-and-delivery scheme," *IEEE Access*, vol. 8, pp. 74349–74358, 2020.

[20] W. Wei, Z. Fuhui, W. Baoyun, W. Qihui, D. Chao, and Q. H. Rose, "Unmanned aerial vehicle swarm-enabled edge computing: Potentials, promising technologies, and challenges," 2022, *arXiv:2201.08517*.

[21] G. A. Vitetta, D. P. Taylor, G. Colavolpe, F. Pancaldi, and P. A. Martin, *Wireless Communications: Algorithmic Techniques*. Hoboken, NJ, USA: Wiley, 2013.

[22] Y. Jiang, *A Practical Guide to Error-Control Coding Using MATLAB*. Norwood, MA, USA: Artech House, 2010.

[23] T. S. Rappaport, *Wireless Communications: Principles and Practice*, vol. 2. Upper Saddle River, NJ, USA: Prentice-Hall, 1996.

[24] M. Ishibashi, M. Umehira, X. Wang, and S. Takeda, "FFT-based frequency domain filter design for multichannel overlap-windowed-DFTs-OFDM signals," in *Proc. IEEE 93rd Veh. Technol. Conf. (VTC-Spring)*, Apr. 2021, pp. 1–5.

[25] T. Okano, M. Umehira, X. Wang, and S. Takeda, "Overlap-windowed-DFTs-OFDM with overlap FFT filter-bank for flexible uplink access in 5G and beyond," in *Proc. IEEE 88th Veh. Technol. Conf. (VTC-Fall)*, Aug. 2018, pp. 1–6.

[26] V. S. Rajput, D. R. Ashok, and A. Chockalingam, "MU-MIMO NOMA with linear precoding techniques in indoor downlink VLC systems," in *Proc. IEEE 91st Veh. Technol. Conf. (VTC-Spring)*, May 2020, pp. 1–6.

[27] S. R. Sabuj, A. Ahmed, Y. Cho, K.-J. Lee, and H.-S. Jo, "Cognitive UAV-aided URLLC and mMTC services: Analyzing energy efficiency and latency," *IEEE Access*, vol. 9, pp. 5011–5027, 2021.

[28] W. Saad, M. Bennis, M. Mozaffari, and X. Lin, *Wireless Communications and Networking for Unmanned Aerial Vehicles*. Cambridge, U.K.: Cambridge Univ. Press, 2020.

[29] F. Silva, R. Feick, R. A. Valenzuela, M. S. Derpich, and L. Ahumada, "Measurement-based evaluation of spectral efficiencies in outdoor-indoor multiuser MISO systems in femto-cells," *IEEE Trans. Wireless Commun.*, vol. 15, no. 9, pp. 5889–5903, Sep. 2016.

[30] I. Hadj-Kacem, H. Braham, and S. B. Jemaa, "SINR and rate distributions for downlink cellular networks," *IEEE Trans. Wireless Commun.*, vol. 19, no. 7, pp. 4604–4616, Jul. 2020.

[31] S. R. Sabuj and M. Hamamura, "Signal technique for friend or foe detection of intelligent malicious user in cognitive radio network," *Int. J. Ad Hoc Ubiquitous Comput.*, vol. 32, no. 1, pp. 29–42, 2019.

[32] J. Choi, J. Kim, J. H. Cho, and J. S. Lehnert, "Widely-linear Nyquist criteria for DFT-spread OFDM of constellation-rotated PAM symbols," *IEEE Trans. Commun.*, vol. 69, no. 5, pp. 2909–2922, May 2021.

[33] H. A. Leftah and M. H. Al-Ali, "Index modulated spread spectrum OFDM with C-transform," *IEEE Commun. Lett.*, vol. 25, no. 9, pp. 3119–3123, Sep. 2021.

[34] R. P. Junior, C. A. F. D. Rocha, B. S. Chang, and D. L. Ruyet, "A novel DFT precoded filter bank system with iterative equalization," *IEEE Wireless Commun. Lett.*, vol. 10, no. 3, pp. 478–482, Mar. 2021.

[35] X. Zhang, Z. Wang, X. Ning, and H. Xie, "On the performance of GFDM assisted NOMA schemes," *IEEE Access*, vol. 8, pp. 88961–88968, 2020.

[36] E. Björnson, J. Hoydis, and L. Sanguinetti, "Massive MIMO networks: Spectral, energy, and hardware efficiency," *Found. Trends Signal Process.*, vol. 11, nos. 3–4, pp. 154–655, Nov. 2017.

[37] P. Singh and A. Trivedi, "NOMA and massive MIMO assisted physical layer security using artificial noise precoding," *Phys. Commun.*, vol. 39, Apr. 2020, Art. no. 100977.

[38] J. Kim, H. Ro, and H. Park, "Deep learning-based detector for dual mode OFDM with index modulation," *IEEE Wireless Commun. Lett.*, vol. 10, no. 7, pp. 1562–1566, Jul. 2021.

JOARDER JAFOR SADIQUE received the B.Sc. (Hons.) and M.Sc. degrees in applied physics and electronic engineering (presently named as electrical and electronic engineering) from the University of Rajshahi, Rajshahi, Bangladesh, in 2010 and 2011, respectively. He has been working as an Assistant Professor with the Department of Electrical and Electronic Engineering, Begum Rokeya University, Rangpur, Bangladesh, since October 2017, where he was a Lecturer, from March 2014 to October 2017. He was also a Faculty Member of the Electrical and Electronic Engineering Department, University of Information Technology and Sciences (UITS), Baridhara, Maddha Nayanagar, Dhaka, Bangladesh, from May 2013 to March 2014. His research interests include 5G/6G compatible mmWave hybrid precoded communications, the Internet of Things (IoT), unmanned aerial vehicle (UAV), cooperative communications, CoMP in MIMO OFDM/OFDMA, channel equalization, and modern channel coding techniques.

SAIFUR RAHMAN SABUJ (Senior Member, IEEE) was born in Bangladesh. He received the B.Sc. degree in electrical, electronic and communication engineering from Dhaka University, Bangladesh, in 2007, the M.Sc. degree in engineering from the Institute of Information and Communication Technology, Bangladesh University of Engineering and Technology, Bangladesh, in 2011, and the Ph.D. degree from the Graduate School of Engineering, Kochi University of Technology, Japan, in 2017. He is currently working as a Postdoctoral Research Fellow with the Electronic Engineering Department, Hanbat National University, South Korea. He has been an Assistant Professor with the Department of Electrical and Electronic Engineering, Brac University, Bangladesh, since September 2017. From 2008 to 2013, he was a Faculty Member of the Green University of Bangladesh, Metropolitan University, Sylhet, and Bangladesh University. His research interests include MIMO-OFDM/NOMA, cooperative communication, cognitive radio, the Internet of Things, unmanned aerial vehicle, and machine-to-machine for wireless communications.

SHAIKH ENAYET ULLAH received the B.Sc. (Hons.) and M.Sc. degrees in applied physics and electronics from the University of Rajshahi, Rajshahi, Bangladesh, in 1981 and 1982, respectively, and the Ph.D. degree from Jahangirnagar University, Dhaka, Bangladesh, in 2000. He is currently a Professor in electrical and electronic engineering with the University of Rajshahi, where he was the Head of the Department of Information and Communication Engineering, from January 2009 to January 2012. He was also the Head of the Department of Applied Physics and Electronic Engineering (Presently named as Electrical and Electronic Engineering), University of Rajshahi, from October 2013 to February 2015. His current research interests include 5G compatible mmWave communications, advanced radio access technology-based, such as NOMA, filter-bank multicarrier (FBMC), index modulation aided OFDM, bi-orthogonal frequency division multiplexing, generalized frequency division multiplexing (GFDM), universal frequency division multiplexing (UFDM), multi-level differential chaos shift keying (DCSK), massive MIMO communications, free space optical communications, cooperative communications, COMP in MIMO OFDM/OFDMA, fading and interference mitigation, and channel equalization and coding.

SUJOY KUMAR JOARDER received the B.Sc. (Hons.) and M.Sc. degrees in information & communication engineering from the University of Rajshahi, Rajshahi, Bangladesh, in 2006 and 2007, respectively. He has over 12 years of professional experience with in-depth knowledge and deep understanding of service delivery regarding ICT hardware, enterprise solutions, consumer electronics appliances, and cellular smartphone networks. During his academic life, he successfully completed some assignments on MATLAB-based simulation of a code division multiple access (CDMA) wireless communication system and investigated its BER/SER performance under both AWGN and fading channel for digital color and monochrome image transmission technique. He has been working as the Head of Service, Samsung at Transcom Electronics Ltd., Dhaka, Bangladesh, since January 2020. Previously, he worked as the Head of Service Operations at Smart Technologies BD Ltd., Dhaka, from June 2010 to January 2020. His current research interests include 5G/6G communications, the Internet of Things (IoT), MIMO OFDM/OFDMA, and modern channel coding techniques.

MASANORI HAMAMURA (Member, IEEE) received the B.S., M.S., and Ph.D. degrees in electrical engineering from the Nagaoka University of Technology, Japan, in 1993, 1995, and 1998, respectively. From 1998 to 2000, he was a Research Fellow of the Japan Society for the Promotion of Science, and from 1998 to 1999, he was a Visiting Researcher with the Centre for Telecommunications Research, King's College London, U.K. From 2017 to 2021, he was the Dean of the School of Informatics, Kochi University of Technology, Japan, and from 2020 to 2021, he was the Chair of IEEE Shikoku Section. He is currently a Professor with the School of Informatics, Kochi University of Technology. He is also serving as the Chair for the IEICE Technical Committee on Wideband Systems (WBS).